



LAWRENCE
LIVERMORE
NATIONAL
LABORATORY

Grain Scale Simulations of Hot-Spot Initiation for Shocked TATB

F. M. Najjar, W. M. Howard, L. E. Fried, M. R.
Manaa, S. Bastea, A. Nichols III

December 9, 2010

ISWI 2010
Cambridge, United Kingdom
September 7, 2010 through September 10, 2010

Disclaimer

This document was prepared as an account of work sponsored by an agency of the United States government. Neither the United States government nor Lawrence Livermore National Security, LLC, nor any of their employees makes any warranty, expressed or implied, or assumes any legal liability or responsibility for the accuracy, completeness, or usefulness of any information, apparatus, product, or process disclosed, or represents that its use would not infringe privately owned rights. Reference herein to any specific commercial product, process, or service by trade name, trademark, manufacturer, or otherwise does not necessarily constitute or imply its endorsement, recommendation, or favoring by the United States government or Lawrence Livermore National Security, LLC. The views and opinions of authors expressed herein do not necessarily state or reflect those of the United States government or Lawrence Livermore National Security, LLC, and shall not be used for advertising or product endorsement purposes.

Grain-Scale Simulations of Hot-Spot Initiation for Shocked TATB

F.M. Najjar¹, W.M. Howard², L.E. Fried², M.R. Manaa², S. Bastea², A. Nichols III²

¹*Weapons and Complex Integration*, ²*Physical and Life Sciences, Lawrence Livermore National Laboratory, 7000 East Avenue, Livermore, CA 94550*
925-423-4479

NAJJAR2@LLNL.GOV

This work was performed under the auspices of the U.S. Department of Energy by Lawrence Livermore National Laboratory under Contract DE-AC52-07NA27344.

Abstract: High explosive shock sensitivity is controlled by a combination of mechanical response, thermal properties, and chemical properties. How these properties interplay in realistic condensed energetic materials is not well understood. In this paper, a multiscale approach is invoked to achieve a realistic simulation of hot spot (void) ignition in a single crystal of the explosive 1,3,5-triamino-2,4,6-trinitrobenzene (TATB). The multiscale procedure links atomistic-based simulations from quantum molecular dynamics with mesoscale simulations from hydrodynamics method. A spherical air bubble is embedded in an insensitive HE and its collapse due to shock initiation is evolved numerically in time.

Keywords: High-Explosives, Multi-scale Analysis, Reactive Flow.

1. Introduction

The collapse of single bubbles in liquid and solid materials has been studied experimentally, theoretically and computationally over the past 100 years. Solid plastic-bonded high-explosive (HE) materials consist of grains that are usually between 10 and 100 microns, with micron-sized embedded impurities and pores. These voids increase the ease of shock initiation by generating high-temperature regions during void collapse that lead to ignition. Bowden & Yoffe [1] systematically studied the role of void collapse. They discuss three key mechanisms of hot spot formation: (i) adiabatic compression of small entrapped bubbles of gas, (ii) friction due to confining surfaces or extraneous grit particles, and intercrystalline friction of the explosive particles, (iii) viscous heating of rapidly flowing explosive material. Starkenberg [2] examined the sensitivity of composition-B (comp-B) and TNT to ignition through vacuum gap tests and investigated bubble radii of 0.7 and 1.5mm. He concluded that heating was the dominant ignition mechanism in situations where large cavities collapsed relatively slowly.

Dear et al. [3] applied high-speed photography and image intensification to study the collapse of cavities by shock waves. They investigated cylindrical cavities of radius 1.5mm embedded in a

gelatine material being impacted by a slider at a shock pressure of 0.26GPa. The configuration included single as well three cavities in tandem. Bourne & Field [4] have performed experiments on two-dimensional bubbles of various shapes, including cylinders, triangles and squares, on the mm to cm length scale. Their measurements based on single-bubble sono-luminescence clearly capture the hydrodynamics of void collapse in single and multiple configurations.

Frey [5] reviewed the theoretical effects concerning the role of voids in explosive initiation and ignition. Mader [6] studied numerically the shock initiation of detonation in nitromethane, liquid TNT and single-crystal PETN. The governing fluid dynamics equations for a reactive material are solved using a one-dimensional Lagrangian finite-difference scheme. The hot spots ranged in size from 0.01 to 0.05cm. Time histories of pressure and temperature are presented and compared to experiments. Carroll & Holt [7] performed computations using a finite-difference hydrodynamic code comparing with theoretical predictions for the pore collapse of a hollow sphere of radius 20 μm and for several porosities.

Tarver *et al.* [8] presented models relevant to chemical kinetic thermal decomposition of pressed HE and accurately computed the time to explosion (TTE) at several initial temperatures comparing with ODTX test for HMX and TATB explosives. Further, they applied their model to higher temperature regimes in order to predict critical temperatures and TTE. They considered void radii of 0.05 μm to 500 μm . Nichols & Tarver [9] enhanced a statistical model for the shock initiation and detonation of HE materials. Their reactive flow model is invoked to predict the onset of hot-spot formation, growth (or failure of) of these hot-spots, rapid transition to detonation and finally yielding to self-sustained detonation. They investigated hot-spots in HMX explosives and considered void radii from 30 μm to 150 μm with shock strengths in the range of 10^{-4} to 1 GPa.

Menikoff [10] performed 2-D simulations for a pore radius of 100 μm embedded in HMX material and interacting with a 13GPa-shock wave. The spatial variation of the temperature is discussed in terms of the shock dynamics and pore collapse. More recently, Tran & Udaykumar [11] have studied numerically void collapse, using a viscoplastic model for the solid high explosive and investigated the collapse mechanism for a radius of 5 μm with and without reactive chemistry. The evolution of the pore shape is discussed for spherical and triangular-shaped voids collapsing in a HMX material. Mintmire *et al.* [12] carried out a series of molecular-dynamics (MD) simulation for a 3D molecular solid using 15056 identical particles and a void radius of 1nm. They highlighted the effects of impact strength on the resulting excitation of the vibrational modes. Recently, McGrane *et al.* [13] have conducted experiments at femtosecond scale on a variety of single-crystal HE materials with micromachined internal voids and showed optical micrographs of the hot spot initiation.

Clearly, understanding the mechanisms of hot-spot initiation in high-explosive materials has had significant research interest in the literature due to safety, reliability and development of new insensitive munitions. In general, the key mechanism leading to explosive initiation has been

proposed to be thermal in its origin. A large number of hot-spot initiation mechanisms have been proposed, including compression of the gases in the voids, elastic-plastic heating of HE materials surrounding the voids, to name a few. The goal of the current study is to investigate the mechanisms of pore collapse and hot spot initiation in simulated TATB crystals. TATB (1-3-5-triamino, 2-4-6-trinitrobenzene) based explosives are an important class of HE due to their insensitivity under thermal and/or shock insults. Compared to conventional HE, e.g. HMX (common name for cyclotetramethylene-tetranitramine), the TATB insensitivity is achieved at a cost of nearly 30% of the total energy and 20% of the detonation pressure (Gustavsen et al., [14]).

The present computational study is performed employing the thermo-hydrodynamics arbitrary-Lagrange-Eulerian code, ALE3D. High-resolution meshes have been employed to properly capture the thermal layers with cells in the nano-meter scale. Prior simulations have not considered the coupling of thermal transport and chemistry to hydrodynamics. Our focus is on the interplay between quantum based reactive dynamics and thermal transport to understand initiation mechanisms in micron-sized voids.

The paper is organized as follows. Section 2 discusses the Molecular Dynamics Quantum computations performed in support of the pore collapse simulations. Section 3 presents the results obtained with the multiphysics code, ALE3D, coupled with the chemical kinetics solver, CHEETAH. Section 4 summarizes the conclusions and provides future work.

2. Molecular Dynamics Quantum Simulations

The smallest length scale (< 10 nm) of the multiscale model was treated quantum mechanically. We have conducted multiple simulations of the decomposition of the explosive TATB using density functional tight binding molecular dynamics (DFTB-MD). The DFTB-MD simulations were conducted for 4, 6, or 8 TATB molecules with periodic boundary conditions imposed. The DFTB-MD simulations are discussed extensively by Manaa et al. [15].

Two types of thermodynamic ensembles were considered in developing a reduced reaction mechanism. In one ensemble, the volume and temperature were held constant throughout the simulation. In the second ensemble, overdriven shock waves were simulated along the intersection of the Rayleigh line and the Hugoniot using the Multi-Scale Shock Technique (MSST) [16]. The MSST self-consistently tracks a small Lagrangian test particle as it propagates through a steady shock wave.

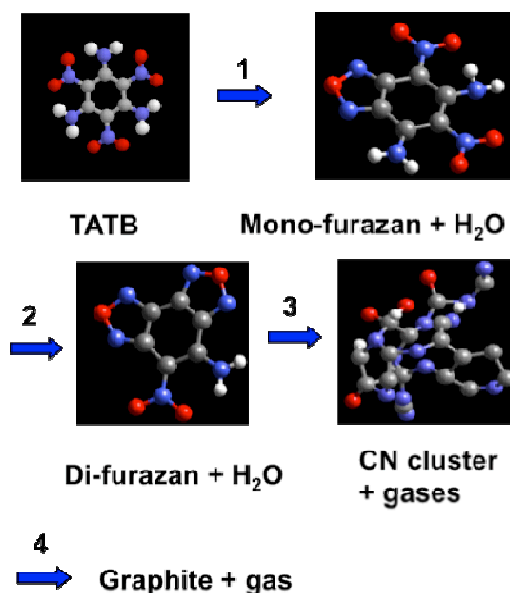
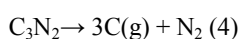
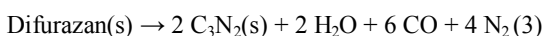
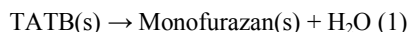


Figure 1: A multi-step mechanism for TATB decomposition at high pressure and temperature was based on quantum simulations.

In our first principles simulations, we found that polymeric nitrogen-rich heterocycles lead to slow reactivity in TATB. This is a novel mechanism for the long reaction zones of carbon-rich explosives [17]. A 4-step reduced chemistry mechanism was matched to the results of the DFTB-MD simulations. The reduced mechanism synthesized from the MD computations is presented schematically in Figure 1. Several experiments have validated water release as one of the early steps in TATB decomposition.

All gases were kept in instantaneous chemical equilibrium using the Cheetah code. The following gases were used in the calculation: N_2 , CO_2 , CH_4 , CO , H_2O , H_2 , NH_3 , HCN , H , NO , N_2O , O_2 , O , N , NO_2 , and C . Enhanced fluid state models of gaseous species including dipolar interactions [18] were used where appropriate. The descriptions of the Cheetah's equation of state are developed for monofurazan, difurazan, and C_3N_2 using a combination of quantum simulations and literature data. C_3N_2 was chosen as a simple representation of the CN bonded clusters found in the first principles simulations. Carbon in the graphite and diamond phase was maintained in instantaneous chemical equilibrium, while the concentrations of TATB, monofurazan, difurazan, and C_3N_2 were controlled by chemical kinetics. For the Cheetah kinetics mechanism, the following reaction set was used:



Arrhenius kinetics were applied for each reaction, such that $dX/dt = -A X \exp(-T_a/T)$ where X corresponds to one of the reactants. Table 1 summarizes the parameters for the Arrhenius reactions.

Reaction	A (μs^{-1})	T_a (K)
1	2.00×10^6	31,000
2	3.21×10^4	17,400
3	7.50×10^5	30,000
4	2.00×10^7	40,000

Table 1. Kinetic parameters for the reduced TATB decomposition mechanism

The kinetic parameters were determined by fitting directly to concentrations obtained from molecular dynamics simulations. Figure 2 presents the concentration of TATB as a function of time at three temperatures of 1500K, 2500K and 3000K. The kinetic mechanism matches quite closely the MD simulations at the higher temperatures of 2500K and 3000K. In addition, the kinetic mechanism predicts very little reaction at 1500K. The MD simulations found no reaction to occur at 1500K for up to 2 ns of simulation time.

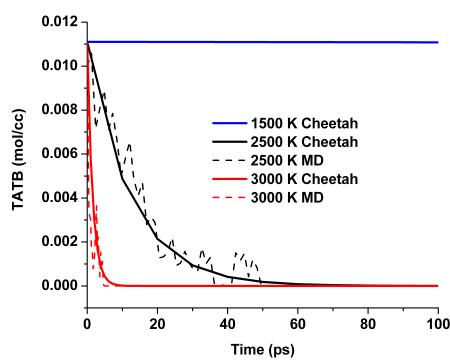


Figure 2: TATB concentration as a function of time compared with MD simulation results.

Figure 3 compares the amount of water produced by the chemical kinetic mechanism with that obtained from the MD simulation. The MD simulations indicate a substantial degree of dissociation of H_2O into H and OH. We found that including H_2O dissociation into the Cheetah model led to numerical convergence difficulties. Therefore, we modeled H_2O as non-dissociating, as typically done in conventional thermochemical treatments of detonation. Bastea & Fried [19] further discuss the dissociation of water in detonation. In order to compare MD simulation results to the non-dissociating kinetics, we compare the sum of the OH and H_2O concentrations obtained by molecular dynamics to the H_2O concentration in the kinetic mechanism.

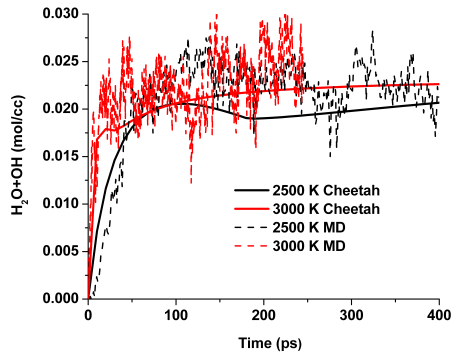


Figure 3: H_2O concentration as a function of time comparing the Cheetah results with MD simulations. For the MD simulations, the sum of the H_2O and OH concentrations is plotted. For Cheetah simulations, only the H_2O concentration is considered.

In Figure 4, we compare the formation of N_2 in the DFTB-MD simulations to that obtained with the reduced kinetic mechanism. It is observed that good agreement is achieved. Further, the mechanisms of N_2 formation occur rarely at the high temperature of 2500K. This leads to a “step” structure in the MD simulation results.

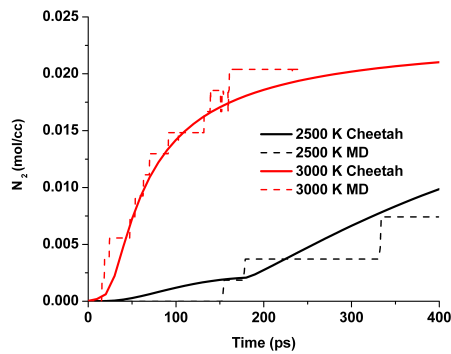


Figure 4: Concentration of N_2 as a function of time for Cheetah and MD simulations.

We derived physics-based descriptions of the thermal transport and heat capacity of each individual species. The thermal conductivity of detonation products was modeled using an effective diameter Enskog theory [19]. We compare the predictions of the modified Enskog theory to experimental data [20] in Figure 5. It is observed that the Cheetah results compare quite well with the experimental measurements.

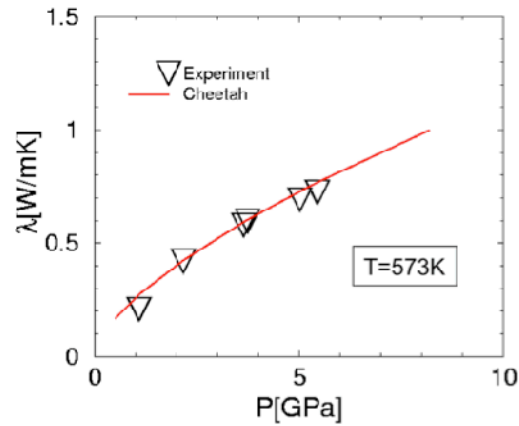


Figure 5: Cheetah models for the thermal conductivity of detonation products were validated against experiment where possible. A comparison of the thermal conductivity of oxygen with Cheetah is shown.

Phonon conduction was assumed to be the dominant thermal conductivity model in solids. A thermal conductivity for solids was based on the relation $\lambda = c_v l u_s / 3$, where λ represents the thermal conductivity, c_v corresponds to the heat capacity, l is the phonon mean path, and u_s is the bulk sound speed. Estimates based on an extended Murnaghan equation of state were determined for each quantity. The computed thermal conductivity for diamond is presented in Figure 6 and is compared to experimental measurements. Again, good agreement is achieved, although the range of experimental data is limited compared to the extremes of conditions in our simulations. Hence, the MD simulations have provided the various parameters needed the chemical kinetics and EOS variables. The next phase of our analysis is to study computationally the pore collapse mechanisms of a spherical air bubble embedded in an insensitive HE material.

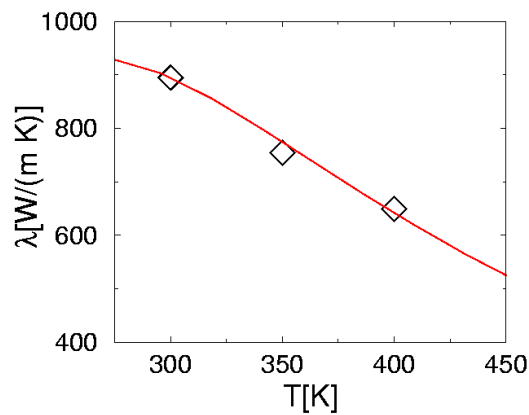


Figure 6: Experimental thermal conductivities for diamond (symbols) are compared against Cheetah code predictions.

3. Hydrodynamics Simulations

The evolution equations for conservation of mass, momentum, energy, thermal diffusion, and chemistry are solved in an Eulerian framework on a structured mesh. A cylindrical axisymmetry was used to optimize computational resources. The multiphysics code, ALE3D [21], was used to perform these simulations and consists several physics modules including hydrodynamics and thermal transport. The mathematical formulation is based on an Operator-Split method and invokes an arbitrary Lagrangian-Eulerian (ALE) approach in two and three-dimensional (3-D/2-D) Cartesian configuration as well as 2-D axisymmetric one.

The capabilities available in ALE3D allow solving the evolution equations either in a pure Lagrangian, pure Eulerian, or in an ALE manner. Within an Eulerian or ALE construct, a remap formalism is invoked, allowing the advection of the conserved variables on the moving mesh. In order to simulate hydrodynamic flow across shock fronts, it is necessary to add some form of numerical dissipation to the conservation equations. This was achieved through the use of artificial dissipation (typically referred to as artificial viscosity) such as the von Neumann-Richtmyer viscosity [22]. Further, to control numerical instabilities due to the finite-element formulation, hour-glass mode control is invoked. Hence, the contributions of artificial viscosity and hour-glass mode control have been included. The governing equations are discretized using a finite-element method and are solved in a weak form. The spatial discretization is of hybrid form where the node coordinates and velocities *are node-centered* variables; while the density, pressure, internal energy, temperature, etc are *cell-centered* quantities. The basis function consists of bi-linear and piecewise constant for the velocities and pressure, respectively. The time integration approach follows a staggered explicit formulation where the velocity fields are computed in a staggered manner from the zonal state variables. Thus, the Lagrangian coordinates, accelerations, pressure, energy, and mass are centered in time at t^n ; while the velocities, are centered in time at $t^{n-1/2}$, where n indicates the time step number. An operator-split scheme is invoked for the hydrodynamics and thermal solvers. An implicit solver was used for the thermal conduction.

The current configuration consists of a continuum material of TATB, where an embedded defect consisting of a spherical air bubble is present. Crystal orientation effects will be considered in future studies. The computational domain consists of a cylindrical section with length and radius, $L = 15 \mu\text{m}$, and $R = 8 \mu\text{m}$, respectively. The dynamics in the neighborhood of the pore were verified to be insensitive to the values of L and R employed. The pore consists of air with a radius, r_p , and is located at the origin along the axis of symmetry. Simulations are conducted using a “reverse ballistic” geometry, where the TATB material collides at a specified velocity v_0 with a fixed wall. The reverse ballistic configuration generates a shock wave that travels from left to right directions through the TATB, collapsing the air bubble. The following boundary conditions are imposed: (i) a reflective left boundary, (ii) non-reflective outflow condition on the right boundary, (iii) with symmetric conditions on the top and bottom. The initial conditions for the simulation are shown schematically in Figure 7.

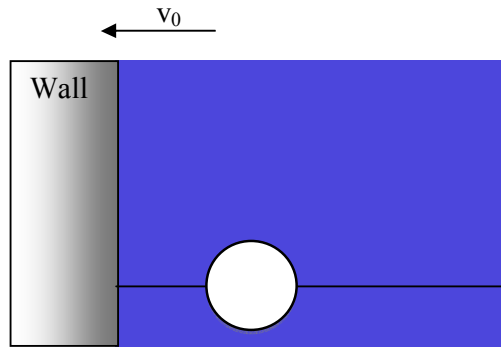


Figure 7: Initial condition for the pore collapse simulation. The axis of symmetry is shown as a black line, TATB is shown in blue color and the air bubble is presented in white. v_0 is the initial velocity for the "reverse ballistic" configuration. For various initial velocities, shocks of different strengths are initiated at the wall, propagation from left to right, collapsing the pore.

Due to the large uncertainties in the strength properties of single crystal TATB, and the relatively high pressures considered here, TATB strength and viscosity were not treated in the present simulations. Future work will explore the effect of strength on the pore collapse dynamics. Multidimensional sparse tables were created in-line during the hydrodynamic simulation by the Cheetah code [24]. The multidimensional tables contained thermal conductivity, heat capacity, and equation of state data. Multistep chemistry was fully coupled to hydrodynamics and heat conduction during the simulation.

The initial velocity field is set to the desired particle velocity in the leftward direction, with atmospheric conditions for the pressure and temperature ($p=1\text{atm}$ and $T=298\text{K}$). The equation of state for air is based on a Quotidian EOS (QEOS) [23]. The 2-D axisymmetric simulations were performed using a 10-nm square mesh size.

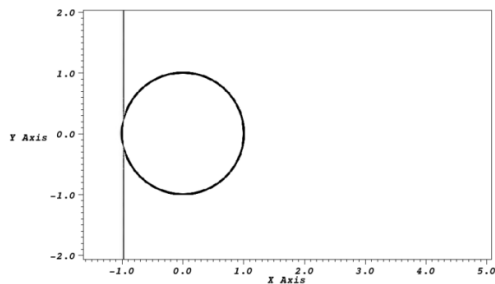
Hydrodynamic simulations of the pore shape were conducted with and without thermal transport. We show simulations with thermal transport included here. The pore shape as a function of time is shown in Figure 8. We find that the spherical void (Fig. 8a) compresses into a primary jet (Fig. 8b). The pore next collapses, lifting from the axis and forming a torus (Fig 8c). Secondary shocks are formed (Fig. 8d), which lead to hot spot formation and collapsed pore convection with rotation (Fig. 8e). Finally the secondary shocks merge onto the axis of symmetry (Fig. 8f).

Our simulations predict several interesting features regarding hot spot dynamics. We find that thermal transport does not significantly change void shape during the compression phase before chemistry begins. On the other hand, temperatures are dramatically affected by thermal transport. Thermal transport between hot compressed air in the pore and the high explosive is found to

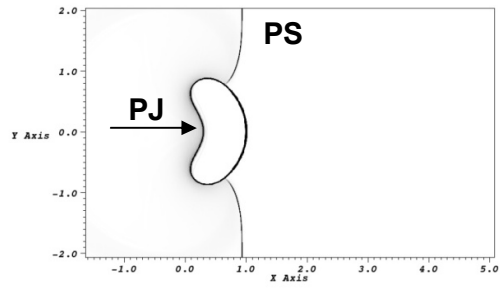
increase the maximum temperature of the high explosive as compared to a system without thermal transport. The thermal transport between the air and the high explosive is enhanced by the formation of a small “secondary jet” which propagates through the hot gas. This distinguishes it from the “primary jet” which is formed when the bubble collapses against the opposite wall of TATB. The secondary jet in a simulation without chemistry is shown in Figure 9.

The reactive simulations predict partial TATB reaction for a wide range of void sizes and shock pressures. We find much less reactivity with a 10-GPa shock pressure than with a 25-GPa shock pressure. Such observation is in rough accord with shock initiation data, which indicates that TATB shock initiation begins at 10 GPa [25]. Many hot spot models, such as that of Nichols, Chidester, and Tarver [8], assume a spherical hot spot ignition locus. Our results (see Figure 10), however, indicate a strong inhomogeneous character to the igniting hot spot, even for a void that is initially spherical. The inhomogeneity is produced by the interaction of several shock waves in the compressing void. We find that the relative importance of igniting regions in transitioning to a steady burn front depends on the strength of the initial shock wave. For stronger shock strengths, there is ignition created by the primary jet when it impacts the opposite wall. This occurs in addition to ignition in the vicinity of the gas bubble. For weaker shock strengths, no ignition at the primary jet location is observed. Although direct comparison to experiment at this scale (several microns) is difficult, our simulations are in reasonable agreement with the experimental shock initiation threshold for TATB.

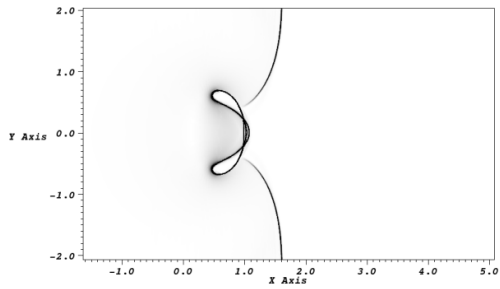
Ignition process is integrated in time over a significant period and various ignition patterns are observed, as shown in Figure 11. Contours of TATB reactants are plotted for two distinct instants of time. The ignited pore is seen convecting in the computational domain. Further, the HE reactants have evolved in time, showcasing the formation of ignition regions, even after the pore has propagated. Rapid formation of TATB reactant material is created due to these ignition processes.



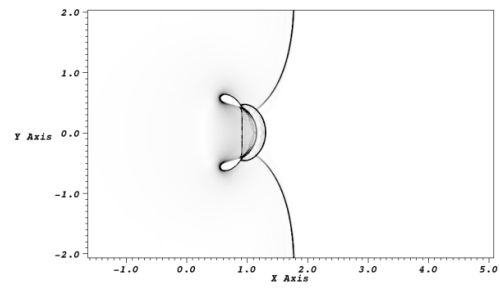
(a)



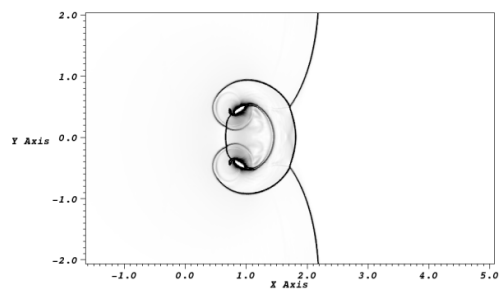
(b)



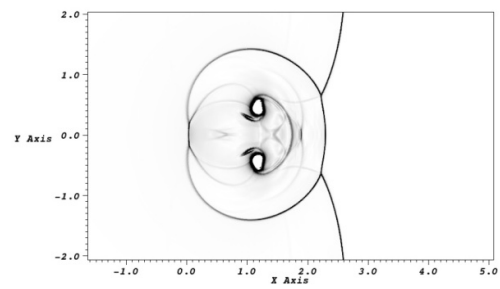
(c)



(d)



(e)



(f)

Figure 8. Contours of numerical Schlieren (corresponding to the magnitude of the density gradient) at representative times for a pore diameter of $1\mu\text{m}$ and a shock strength of 6GPa: (a) at shock impact; (b) creation of primary jet (PJ). The primary shock (PS) is also shown; (c) pore collapse; (d) formation of secondary shocks; (e) hot spot formation ; (f) merging of secondary shocks onto axis of symmetry. Contour levels are $[0,5] \text{ g/cm}^4$. Distances are shown in μm .

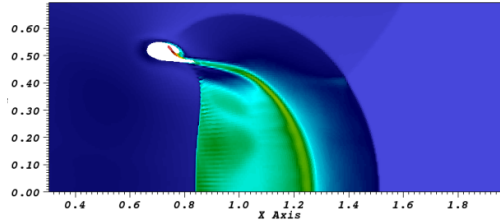
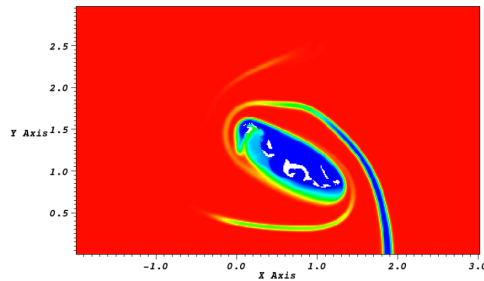
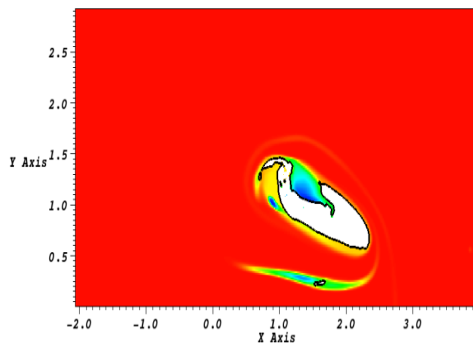


Figure 9: Pore collapse leads to TATB being injected into hot air. This dramatically increases the temperature of the TATB. We term this ignition mechanism a “secondary jet”. Color contours show the range 300K (dark blue) to 5000K (red). Distances are shown in μm units. The axis of symmetry is shown at $y = 0$.



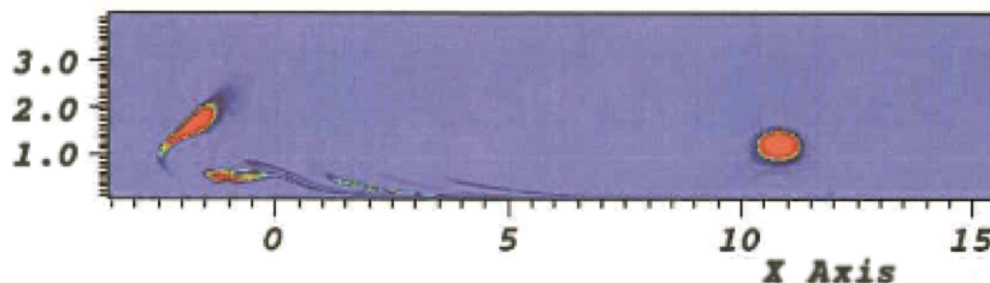
(a)



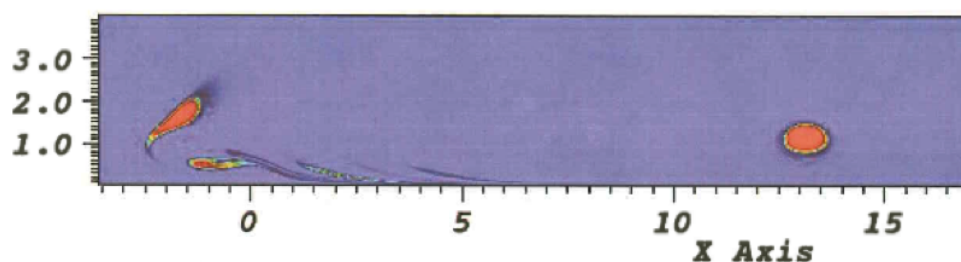
(b)

Figure 10: Contour levels of TATB concentration around a 4-micron diameter compressed void. Red (blue) corresponds to a mass fraction of TATB products for a value of 1.0 (0.0). This means that blue contours represents products of the chemical reactions. Distance is shown in microns. The simulation is cylindrically symmetric about the x-axis. (a) a 25-GPa shock, (b) a 10-GPa

shock. In the bottom frame, the air-TATB interface is outlined in black for clarity. Ignition locations are found in several positions around the void. Color contours are in the range of 0 (blue) to 1 (red).



(a)



(b)

Figure 11: Contour levels of TATB reactants following the 4- μm diameter pore collapse due a 25-GPa shock. Blue (red) corresponds to mass fraction of TATB reactants for a value of 0.0 (1.0). TATB regions are ignited substantially even after the pore has collapsed and dissipated. Two representative instants of time are shown at (a) $t=10.1$ ns, and (b) $t=11.9$ ns.

4. Conclusions

We can analyze the ignition process and growth from our simulations by plotting the TATB mass fraction for the entire computational domain as a function of time. Results are shown in Figure 12. We find significantly more reaction for a 25-GPa shock than one for a 10-GPa shock. Further, we find that the degree of reaction depends sensitively on void size. We found that a 2- μm diameter void is much less effective at inducing TATB reactivity than a 4- μm diameter void.

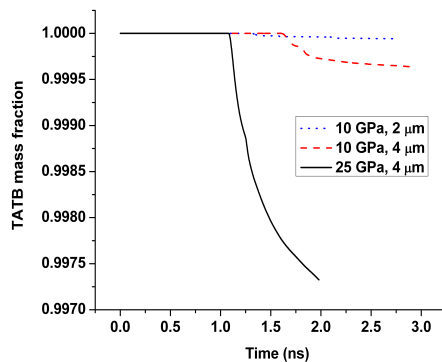


Figure 12: Total mass fraction of TATB in the simulation system as a function of time for different shock strengths and pore diameters.

In summary, this paper describes the first quantum-based multi-scale simulation of hot spot ignition using realistic equations of state, chemistry, and thermal transport properties. Our results indicate a complex mechanism for pore ignition than one that is usually considered in macroscopic shock initiation models, and an unexpected sensitivity to thermal transport in secondary jets. Further work is underway to develop an ignition term for use in reactive flow models that is consistent with our results.

References

1. Bowden, F. P. and Yoffe, A. D., Initiation and Growth of Explosions in Liquids and Solids, Cambridge University Press, New York, 1951.
2. Starkenberg, J., Seventh Symposium (International) on Detonation, White Oak, MD, pp. 3, 1982.
3. Dear, J. P., Field, J.E. and Walton, A.J. *Nature*, Vol. 332, pp. 505, 1988.
4. Bourne, N.K., and Field, J.E., *Phil. Trans.: Math, Phys. And Eng. Sciences*, Vol. 357, pp. 295, 1999.
5. Frey, R.B. Eighth Symposium (International) on Detonation, White Oak, MD, pp. 385, 1985
6. Mader, C.L., *Phys. Fluids*, Vol. 6, pp. 375 (1963)
7. Carroll, M.M. and Holt, A.C., *J. Appl. Phys.* Vol. 43, pp. 1626, 1972.
8. Tarver, C.M., Chidester, S.K. and Nichols, A.L. III, *J. Phys Chem.*, Vol. 10, pp. 5794, 1996.
9. Nichols, A.L. III and Tarver, C.M., Twelveth International Detonation Symposium, San Diego, CA, 2002.
10. Menikoff, R., Shock Compression of Condensed Matter, Vol. 393, 2003.
11. Tran, L., and Udaykumar, H.S., *J. Prop. Power*, Vol. 22, pp. 947, 2006; Tran, L., and Udaykumar, H.S., *J. Prop. Power* Vol. 22, pp. 959, 2006.
12. Mintmire, J.W. Robertson, D.H. and White, C.T., *Phys. Review B* Vol. 49, pp. 14859, 1994.
13. McGrane, S.D., Grieco, A., Ramos, K.J., Hooks, D.E., and Moore, D.S., *J. Appl. Phys.* Vol. 105, art. 073505, 2009.
14. Gustavsen, R.L., Sheffield, S.A. and Alcon, R.R., *J. Appl. Phys.*, Vol. 99, pp. 114907, 2006.
15. Manaa, M. R., Reed, E. J. and Fried, L. E., "Atomistic simulations of chemical reactivity of TATB under thermal and shock conditions", 14th Symposium (International) on Detonation.
16. Reed, E. J., Fried, L. E. and Joannopoulos, J., "A method for tractable studies of single and double shock compression", *Phys. Rev. Lett.*, Vol. 90, art. 235503, 2003.
17. Manaa, M. R., Reed, E. J., Fried, L. E. and Goldman, N., "Nitrogen-rich heterocycles as reactivity retardants in shocked insensitive explosives", *Journal of the American Chemical Society*, Vol. 131, pp. 5483-5487, 2009.
18. Bastea, S. and Fried, L. E., "Exp6-polar thermodynamics of dense supercritical water", *J. Chem. Phys.* Vol. 128, pp. 174502, 2008.

19. Bastea, S. and Fried, L. E., "Major effects in the thermodynamics of detonation products: Phase segregation versus ionic dissociation", 14th Symposium (International) on Detonation, 2010.
20. Abramson, E. H., Slutsky, L. J. and Brown, J. M. , "Thermal diffusivity of fluid oxygen to 12 GPa and 300 C", J. Chem. Phys., Vol. 111, pp. 9357, 1999.
21. Nichols A. L. III, Editor, "User's Manual for ALE3D, An Arbitrary Lagrange/Eulerian 2D and 3D Code System", Lawrence Livermore National Laboratory, LLNL-SM-404490 Rev. 1, 2009.
22. von Neumann, J., and Richtmyer, R.D. , *J. Appl. Phys.*, Vol. 21, pp. 232, 1950.
23. More, R.M, Warren, K.H., Young, D.A. and Zimmerman, G.B., *Phys Fluids*, Vol. 31, pp. 3059,1988.
24. Vitello, P., Fried, L. E., Pudliner, B. and McAbee, T., "Sparse partial equilibrium tables in chemically resolved reactive flow", in *Proceedings of the 2003 APS Conference on Shock Compression of Condensed Matter*, Portland, OR., AIP Conference Proceedings Vol. 706, pp. 1061, 2003.
25. Vandersall, K. S., Garcia, F. and Tarver, C. M. , "Shock Initiation experiments on the TATB based explosive RX-03-GO with ignition and growth modeling", *Shock Compression of Condensed Matter, 2009*, ed. M. L. Elert, W. T. Butler, M. D. Furnish, W. W. Anderson, and W. G. Proud, AIP Conference Proceedings 1195.